Int. J. Heat Mass Transfer. Vol. 36, No. 18, pp. 4419–4431, 1993
Printed in Great Britain

0017–9310/93 $6.00 + 0.00

High pressure droplet vaporization; effects of liquid-phase gas solubility

H. JIA
Department of Mechanical and Aerospace Engineering, Rutgers University, P.O. Box 909, Piscataway, NJ 08855-0909, U.S.A.
and
G. GOGOS†
Department of Mechanical Engineering, University of Nebraska–Lincoln, Lincoln, NE 68588-0656, U.S.A.

(*Received* 10 *December* 1992 *and in final form* 18 *May* 1993)

Abstract—Numerical results are presented for an *n*-hexane droplet initially at 300 K evaporating into nitrogen, for ambient pressures, P_∞, 1–100 atm and ambient temperatures, T_∞, 500–1500 K. At low P_∞ (< 30 atm), droplet lifetimes predicted with or without liquid-phase gas solubility are very close. At high P_∞, the model neglecting solubility either underestimates the droplet lifetime (low T_∞) or breaks down by failing to predict vapor–liquid equilibria (high T_∞). At high enough P_∞, heat-up is extremely important throughout the entire droplet lifetime. In a fuel rich environment, relatively low T_∞ and high P_∞, substantial condensation occurs before the onset of vaporization.

1. INTRODUCTION

IT HAS been established experimentally [1–5] that during spray combustion the center of the spray remains relatively cool and too fuel rich. As a consequence, droplets simply evaporate in the interior of the spray, without undergoing fuel oxidation and/or decomposition [6]. In devices such as liquid-fueled rocket engines and diesel engines, the evaporation of the droplets takes place within a high pressure environment. Under these conditions of elevated pressures, many effects that are assumed negligible at low and moderate ambient pressures become very important. Solubility of the ambient gas into the liquid phase is one of these effects. Its importance increases with increasing ambient pressure and is the main focus of the present study.

Various aspects of high pressure droplet vaporization have been examined under the assumption that the ambient gas does not dissolve in the liquid droplet [7–12]. Of particular relevance to the present study are the works on spherically symmetric high pressure droplet vaporization that have addressed the problem of gas solubility [13–19]. Manrique and Borman [13] were the first to consider solubility of the inert gas in the liquid phase in a numerical study of liquid carbon dioxide droplets evaporating in nitrogen at high ambient pressures (70–120 atm). In addition, their model included the effects of non-ideal mixtures, variation of transport properties and non-ideality of the energy required for phase change. They found that at sufficiently high pressures, steady state conditions cannot be attained. Their calculations showed that the droplet vaporization rate increases with increasing pressure. However, the heat-up of the droplet interior has been neglected (although at elevated pressures it remains important throughout the entire droplet lifetime), the gas-phase was treated as quasi-steady, and solubility was examined in the limiting case where absorption of nitrogen into the liquid phase was assumed to be confined to a thin layer at the droplet surface. Lazar and Faeth [14] investigated high pressure droplet combustion of *n*-octane and *n*-decane droplets in air. They developed a theoretical high pressure model which allows for real gas effects as well as finite ambient gas solubility. This study also neglected heat-up of the droplet interior, assumed quasi-steady gas phase and considered limiting cases of liquid-phase gas solubility. Predicted conditions for supercritical burning agreed reasonably well with measured ones. Canada and Faeth [15] employed a high pressure model as well as a conventional low pressure approach and predicted droplet burning-rates for a number of liquid fuels. The burning-rate predictions of the two models were similar, and in fair agreement with their experimental data. Curtis and Farrell [16, 17] developed a high pressure model that predicts droplet vaporization rate, droplet temperature and the critical mixing state. They found that anomalies in the transport properties of a fluid near its critical mixture point are insignificant in droplet vaporization under conditions similar to those in a diesel engine. Hsieh *et al.* [18] developed a comprehensive model on high pressure droplet vaporization considering real gas effects as well as ambient gas solubility. Results were presented for an ambient temperature of 2000 K and it was predicted that the droplet evaporation rate increases progressively with pressure. In a more recent study Delplanque and Sirignano [19] developed an elaborate numerical model to investigate transient vaporization of a liquid oxygen droplet in gaseous hydrogen at moderate and high pressures. It was shown that under supercritical pressures the droplet

† Author to whom correspondence should be addressed.

NOMENCLATURE

a, b	parameters in Peng–Robinson equation
c_p	specific heat at constant pressure
D_0	initial droplet diameter
D_{12}	binary mass diffusion coefficient
f_i	fugacity of the ith species
H_i	molar enthalpy of the ith species
$\bar{H}_i$	partial enthalpy of the ith species
k	thermal conductivity
m	instantaneous droplet mass
m_i	mass fraction of the ith species
$\dot{m}''$	mass flux of vaporization at interface
n_i	number of moles of the ith species
P	pressure
q	energy transported at interface
r	radial coordinate
R	instantaneous radius of the droplet
R_u	universal gas constant
$\dot{R}$	regression rate of the droplet surface
t	time
T	temperature
V	total volume of the mixture
v	specific volume of the mixture
v_r	radial velocity
x	mole fraction in liquid phase
y	mole fraction in gas phase.

Greek symbols

β	evaporation constant
Δc_p	departure function for heat capacity
Δh	energy required for phase change
μ	viscosity
ρ	density
τ	dimensional droplet lifetime
ϕ_i	fugacity coefficient of the ith species.

Subscripts

0	initial condition
g	gaseous phase
i	ith species
l	liquid phase
s	droplet surface
vp	saturated vapor pressure
∞	ambient conditions.

Superscripts

0	ideal gas
l	liquid phase
sat	saturated conditions
v	vapor.

surface temperature reaches the computed critical mixture value and it was suggested that a model for supercritical combustion is needed.

The goal of the present study is to examine various aspects that add tremendously to the complexity and uncertainty of a comprehensive high pressure droplet vaporization model. There is a need for such an elaborate model, yet it must be of moderate complexity so that it can be used in a large spray code [11, 19]. First, the importance of dissolved ambient gas into the liquid droplet needs to be examined. Allowing for gas solubility in the droplet interior makes the calculation for the vapor–liquid equilibrium composition and for the energy required for phase change at the droplet surface extremely complex. Furthermore, the species equation in the liquid phase needs to be solved. In addition to the complexity, the limited information on binary diffusion coefficients in the liquid phase, and the use of the equation of state in the liquid phase for composition calculations at the droplet surface add uncertainties to the model. Therefore, it is highly desirable to know the range of ambient conditions where a simplified model can be employed. In view of this, both a comprehensive model that allows for solubility and a simplified model that neglects gas solubility in the droplet interior have been developed in the present study; comparison between the two models identifies the range of ambient pressures and temperatures where the simplified model would be of adequate accuracy. Second, the solution of the pressure field using both the ICE algorithm [20, 21] and a pressure gradient scaling technique [22] is obtained in order to examine the validity of the constant pressure assumption. The present study provides an exhaustive presentation of the droplet lifetime dependence on ambient pressure and temperature. The important role that the liquid-phase heat-up plays on the droplet lifetime with increasing pressure is clearly delineated. In addition, for a fuel rich environment, low ambient temperature, and high ambient pressure, conditions which may be simulating the core of the spray, it is predicted that significant condensation occurs during the early part of the droplet lifetime which may increase the droplet mass substantially.

2. PROBLEM FORMULATION

A liquid fuel droplet of initial radius R_0 is evaporating within a stagnant inert environment of infinite expanse. The initial temperature of the droplet is T_0 and the ambient pressure and temperature are P_∞ and T_∞ respectively.

Since the study is focused on high pressure effects, natural convection is neglected, rendering the problem spherically symmetric. Moreover, spherically symmetric vaporization at elevated pressures may be of practical interest in microgravity environments.

Consequently, the only convective motion present in the gas phase is that induced by vaporization which causes a radial flow field in the gas phase. Changes in the liquid phase density both due to thermal expansion and change in species composition contribute to the rate at which the droplet surface is receding and are incorporated in the model. In the analysis that follows, subscripts 1 and 2 refer to the vaporizing fuel species and the inert gas initially present only in the gaseous phase. The following assumptions are employed: (a) the droplet shape remains spherical, (b) radiation is negligible, (c) second order effects such as the Soret and Dufour effects are negligible, and (d) viscous dissipation is neglected. With these assumptions, the governing conservation equations in spherical coordinates are:

For the gaseous phase, $r > R(t)$

continuity equation

$$\frac{\partial(\rho r^2)}{\partial t} + \frac{\partial}{\partial r}(\rho r^2 v_r) = 0 \tag{1}$$

species equation

$$\frac{\partial(\rho r^2 m_1)}{\partial t} + \frac{\partial(\rho r^2 v_r m_1)}{\partial r} = \frac{\partial}{\partial r}\left(\rho D_{12} r^2 \frac{\partial m_1}{\partial r}\right) \tag{2}$$

energy equation

$$\frac{\partial(\rho r^2 T)}{\partial t} + \frac{\partial(\rho r^2 v_r T)}{\partial r} = \frac{1}{c_p}\frac{\partial}{\partial r}\left(k r^2 \frac{\partial T}{\partial r}\right) + \frac{\rho r^2 D_{12}}{c_p}\frac{\partial T}{\partial r}(c_{p1} - c_{p2})\frac{\partial m_1}{\partial r} + \frac{v_r r^2}{c_p}\frac{\partial P}{\partial r} \tag{3}$$

momentum equation

$$\frac{\partial(\rho r^2 v_r)}{\partial t} + \frac{\partial(\rho r^2 v_r^2)}{\partial r} = \frac{\partial}{\partial r}\left(\frac{4}{3}\mu r^2 \frac{\partial v_r}{\partial r}\right) - \frac{8}{3}\mu v_r - \frac{4}{3} v_r r \frac{\partial \mu}{\partial r} - r^2 \frac{\partial P}{\partial r}. \tag{4}$$

In the above equations, t and r refer to temporal and spatial variables, R is the instantaneous radius of the droplet, T is the temperature, ρ, k, μ and c_p are the density, thermal conductivity, viscosity and specific heat at constant pressure of the gaseous mixture, v_r is the radial velocity induced by vaporization, m_1 is the fuel vapor mass fraction, D_{12} is the binary mass diffusion coefficient, c_{p1} and c_{p2} are the specific heats at constant pressure for pure species 1 and 2 and P is the pressure.

For the liquid phase, $r < R(t)$

energy equation

$$\frac{\partial(\rho r^2 T)}{\partial t} = \frac{1}{c_p}\frac{\partial}{\partial r}\left(k r^2 \frac{\partial T}{\partial r}\right) + \frac{\rho r^2 D_{12}}{c_p}\frac{\partial T}{\partial r}(c_{p1} - c_{p2})\frac{\partial m_1}{\partial r} \tag{5}$$

species equation

$$\frac{\partial(\rho r^2 m_1)}{\partial t} = \frac{\partial}{\partial r}\left(\rho D_{12} r^2 \frac{\partial m_1}{\partial r}\right). \tag{6}$$

The boundary conditions are:

At the droplet center:

$$\frac{\partial T}{\partial r} = 0 \quad \text{and} \quad \frac{\partial m_1}{\partial r} = 0. \tag{7}$$

As $r \to \infty$:

$$T \to T_\infty \quad \text{and} \quad m_1 \to m_{1,\infty}, \tag{8}$$

$$P \to P_\infty \quad \text{and} \quad v_r \to 0. \tag{9}$$

At the droplet surface:

mass conservation

$$\dot{m}'' = \rho_g(v_{r,g} - \dot{R}) = \rho_l(v_{r,l} - \dot{R}) \tag{10}$$

species conservation

$$(m_{1,l} - m_{1,g})\dot{m}'' - \rho_l D_{12,l}\frac{\partial m_{1,l}}{\partial r} + \rho_g D_{12,g}\frac{\partial m_{1,g}}{\partial r} = 0 \tag{11}$$

temperature continuity

$$T_g = T_l \tag{12}$$

energy conservation

$$\sum_{i=1,2}\left(\dot{m}'' m_{i,g} - \rho_g D_{12,g}\frac{\partial m_{i,g}}{\partial r}\right)(\bar{H}_{i,g} - H_{i,l}) + k_l\frac{\partial T_l}{\partial r} - k_g\frac{\partial T_g}{\partial r} = 0 \tag{13}$$

vapor–liquid equilibrium relationships (to be discussed in more detail later in this section)

$$m_i = m_i(T_s, P) \quad i = 1, 2. \tag{14}$$

The overall mass-conservation condition which determines the rate of change of the droplet radius is given by:

$$-\rho_l(R,t)\dot{R} = \dot{m}'' + \int_0^{R(t)}\left(\frac{r}{R}\right)^2\frac{\partial\rho(r,t)}{\partial t}\,dr. \tag{15}$$

In the above equations $\dot{m}''$ is the mass flux at the droplet surface, subscripts g and l indicate gas side and liquid side at the droplet interface, respectively, subscript s indicates the droplet surface, $\bar{H}_i$ and H_i are the partial and molar enthalpies of the ith component and $\dot{R}$ is the regression rate of the droplet surface. Equation (15) indicates that the rate at which the droplet surface is receding depends on both the rate of mass loss (gain) due to evaporation (condensation), and the change in the liquid phase density due to thermal expansion and change in species composition (second term on the right hand side).

In addition to the above equations, an equation of

state needs to be used. To capture the real gas behavior of the gas phase at high pressures and predict liquid–vapor equilibrium composition at the droplet surface, the Peng–Robinson equation of state [23] is employed. This equation is superior than the widely used Redlich–Kwong equation in calculating specific volumes both for liquid and gas mixtures [23–25]. The Peng–Robinson equation of state is given in the form:

$$P = \frac{R_u T}{v-b} - \frac{a}{v(v+b)+b(v-b)} \tag{16}$$

where v is the specific volume of the gaseous mixture, R_u is the universal gas constant, and a and b are the two parameters. For pure compounds, the parameter a is a function of temperature and acentric factor and b is a constant. For mixtures both parameters a and b are composition dependent through the mixing rules proposed in ref. [23]. It can be easily shown that equation (16) is a cubic polynomial in v. Its largest and smallest real roots provide the specific volume v of the gaseous and liquid mixture, respectively.

In the next few paragraphs the vapor–liquid equilibrium relationships, the critical state for binary systems, the energy required for change of phase and the transport and thermodynamic properties are discussed.

The liquid and gas phase composition at the droplet surface is calculated by assuming thermodynamic equilibrium. In addition to the temperature and pressure being equal, the fugacity of each species at the liquid phase is equal to the fugacity of the same species in the gas phase, namely:

$$f_i^v = f_i^l, \quad i = 1, 2 \tag{17}$$

where superscripts v and l indicate vapor and liquid phase, respectively. The fugacity coefficients, $\phi_i^v = f_i^v/y_i P$ and $\phi_i^l = f_i^l/x_i P$, are introduced to relate y_i and x_i, the mole fractions of the ith species in gas and liquid phase, respectively, to the fugacities of each species in both phases. The fugacity coefficient, ϕ_i, is a function of pressure, temperature, and composition and is provided by the following thermodynamic relation in terms of the volumetric properties of the mixture:

$$R_u T \ln \phi_i = \int_v^\infty \left[\left(\frac{\partial P}{\partial n_i} \right)_{T,v,n_j} - \frac{R_u T}{v} \right] dv - R_u T \ln z \tag{18}$$

where z is the compressibility factor and n_i is the number of moles of the ith species. By substituting the Peng–Robinson equation with the proper mixing rules [23], the fugacity of the ith component in the liquid and gaseous mixture is given by [24]:

$$\ln \phi_i = \frac{b_i}{b R_u T}(Pv - R_u T) - \ln\left[\frac{P}{R_u T}(v-b)\right] - \left[\frac{a}{2\sqrt{2} b R_u T}\right]\left[\frac{2\sum_{j=1}^{N} y_j a_{ij}}{a} - \frac{b_i}{b}\right] \times \ln\left[\frac{v+(1+\sqrt{2})b}{v+(1-\sqrt{2})b}\right]. \tag{19}$$

The binary interaction coefficient needed for equation (19) was taken from Knapp *et al.* [24]. Equations (17)–(19) provide the pair of vapor–liquid equilibrium relationships indicated in equation (14). It is a system of two lengthy highly nonlinear algebraic equations that need to be solved iteratively at each time step. Its solution provides both the liquid and the gas phase equilibrium composition for the comprehensive model. However, for the simplified model where solubility of the inert gas in the liquid phase is neglected, equation (14) reduces to a single vapor–liquid equilibrium relationship, which takes the form [12]:

$$y_1(P, T) = \frac{P_{vp,1}(T)}{P} \frac{\phi_1^{sat}(T)}{\phi_1} \exp\left(\int_{P_{vp,1}}^{P} \frac{v_1^l(T, P)}{R_u T} dP \right) \tag{20}$$

where $P_{vp,1}$ is saturated pressure of pure fuel vapor at temperature T, v_1^l is its liquid molar volume and ϕ_1^{sat} is fugacity coefficient at saturated conditions given by $f_1^{v,sat}/P_{vp,1}$. Both $P_{vp,1}$ and ϕ_1^{sat} are functions of temperature only. The liquid molar volume changes weakly with pressure and is approximated by the molar volume of the saturated liquid at the same temperature, namely, $v^l(P, T) \simeq v^l(T)$. Neglecting solubility imposes further simplifications. The species equation in the liquid phase, equation (6), need not be solved. It is highly desirable to clearly delineate the range of ambient pressures and temperatures where equation (6) may be dropped, since there is very little experimental data on liquid phase mass diffusion coefficients.

The critical state of a multi-component system, namely, the critical temperature, pressure and a specific volume, can be obtained rigorously by applying the Gibbs criteria of stability to such a system [26–28]. For a binary system, the criteria of stability take the following form [26, 27]:

$$\frac{\partial^2 G}{\partial n_1^2} = 0 \quad \text{and} \quad \frac{\partial^3 G}{\partial n_1^3} = 0 \tag{21}$$

where G is the Gibbs free energy. The above two equations can be expressed in terms of partial derivatives for Helmholz free energy A through the thermodynamic relation, $G = A + PV$, where V is the total volume of the mixture. The Helmholz free energy is related to the fugacity through the following thermodynamic equations [28]:

$$\frac{\partial^2 A}{\partial n_1^2} = R_u T \frac{\partial \ln f_1}{\partial n_1} \quad \text{and} \quad \frac{\partial^3 A}{\partial n_1^3} = R_u T \frac{\partial^2 \ln f_1}{\partial n_1^2}. \tag{22}$$

Using equations (22) together with the equation of state, Gibbs criteria of stability are expressed in terms

of the state properties of the mixture. Thus, given the composition of a binary system, the critical points T_c, P_c and v_c, can be obtained by solving simultaneously equations (16) and (21). Using this approach, the calculated critical points are more accurate than those predicted by any empirical correlations [25].

Deviation between the usually assumed latent heat of vaporization for pure component and the enthalpy required for vaporization into a gas mixture is determined by employing the Peng–Robinson equation of state. The energy required for phase change, Δh, is given by:

$$\Delta h = \sum_{i=1,2} x_i \bar{H}_i(T, P, y_i) - \sum_{i=1,2} x_i H_{i,l}(T, P). \quad (23)$$

The partial enthalpy $\bar{H}_i$ of component i and its ideal gas enthalpy H_i^0 at the same temperature are related through the thermodynamic relation:

$$(\bar{H}_i - H_i^0)_T = -R_u T^2 \left(\frac{\partial \ln \phi_i}{\partial T}\right)_{P,x} \quad (24)$$

where

$$H_i^0(T) = \int_{T_0}^{T} c_{pi}^0 \, dT \quad (25)$$

and c_{pi}^0 is the specific heat at constant pressure for ideal gas.

The heat capacity at constant pressure of a real gas is given by:

$$c_p = \sum_{i=1}^{N} y_i c_{pi}^0 + \Delta c_p \quad (26)$$

where superscript 0 indicates ideal gas and the residual heat capacity, Δc_p, is obtained using the Peng–Robinson equation of state as recommended by Reid *et al.* [25].

The gas phase transport and thermodynamic properties are considered varying with temperature, pressure and composition. The binary mass diffusion coefficient D_{12} is calculated based on the theory of Chapman and Enskog, with collision integral given in ref. [29]. Then, the Takahashi correlation [30] is used to correct for high pressure effect on D_{12}. The thermal conductivity and viscosity for pure components are obtained using the correlations by Chung *et al.* [31, 32], and are corrected for high pressure effect by the method of Chung *et al.* [31, 32]. The high pressure mixing rule recommended in refs. [31, 32] is employed to calculate k and μ for the binary mixture at high pressures. All the methods employed for the calculation of the transport properties are recommended by Reid *et al.* [25].

The liquid phase properties are evaluated as functions of temperature and composition only. The liquid densities of *n*-hexane and nitrogen are given by Canjar and Manning [33] and Reynolds [34], respectively. The density of the mixture is obtained through mass fraction weighting. The liquid heat capacities are given by Bondi [35] and Rowlingson [36] and the liquid phase diffusion coefficient by Nakanishi [37]. The Sato–Riedel [38] correlation is employed for the calculation of liquid thermal conductivities for pure components, and the Filippov [39] correlation is used to obtain k for the liquid mixture.

3. METHOD OF SOLUTIONS

Solutions to the model are pursued in a spatial coordinate system given by $r^* = r/R$ in the liquid phase and $r^{**} = \ln(r/R)$ in the gaseous phase, where $0 \leqslant r^* \leqslant 1$ and $0 \leqslant r^{**} < \infty$. In view of the above coordinate transformation, using a constant step size Δr^{**}, grid points in the gaseous phase are clustered close to the droplet interface where gradients are steep. Furthermore, the gas-phase outer boundary in the physical domain can be kept far away from the droplet surface with a small number of grid points leading to efficient computing.

The fully implicit scheme (backward-time, central-space) was utilized to discretize the governing equations and boundary conditions [40]. All variables are solved iteratively within one time step and the procedure is given as follows. Properties of liquid and gaseous phase are calculated at the temperature, pressure and composition from the previous time step or iteration. Then, the droplet surface quantities $\dot{m}''$, $\dot{R}$ and $v_{r,g}$ are calculated through equations (10), (11) and (15), respectively. Next, the temperature and composition of both phases are solved in a tridiagonal matrix form using equations (2), (3), (5), (6) and the relevant boundary conditions (7), (8) and (12)–(14). Then, the liquid density is calculated. The ICE scheme [20, 21] is employed to solve for P, ρ and v_r using equations (1), (4), (16) and (9). The pressure field is obtained by the pressure gradient scaling technique that was developed by Ramshaw *et al.* [22] for fluid flows with nearly uniform pressure. The solution is obtained in terms of a new variable $\alpha^2(P - P_\infty)$, where $\alpha > 1$, provided $\alpha^2(P - P_\infty) \ll P_\infty$. By introducing such a scaling factor, the pressure field, which is nearly uniform in the radial direction, can be solved with much improved accuracy and the poor coupling between the momentum equation and the rest of the governing equations is reduced. In addition, staggered grid points are employed. Finally, the criterion for convergence is checked before the calculation advances to the next time step and the radius of the droplet is updated.

For the gas phase, a step function is used as initial condition for temperature. Solutions invariant with step size are obtained by changing the step size. Variable time steps are employed to improve the computing accuracy and efficiency. Calculations are terminated when $(R/R_0)^2 < 0.2$, or when the critical state for the binary system is reached.

4. RESULTS AND DISCUSSION

Results for a *n*-hexane droplet evaporating into a nitrogen environment will be presented later in this

section. Before these results are presented, several key aspects of our model, such as the thermodynamic equilibrium and the energy required for phase change at the droplet surface are discussed.

As was discussed earlier, an equation of state is needed to calculate the vapor–liquid equilibrium composition for a binary system. Most previous studies [7, 10–16, 19] have employed the modified Redlich–Kwong equation developed by Chueh and Prausnitz [41]. Recently, some researchers [17, 18] have been using the Peng–Robinson [23] or the Soave–Redlich–Kwong [42] equations, which have been shown to be more accurate than the Redlich–Kwong equation in predicting vapor–liquid equilibrium over a wide pressure range [25]. To choose a suitable equation of state for our model, all three previously mentioned equations are compared with the experimental data for an *n*-hexane–nitrogen system in thermodynamic equilibrium obtained by Poston and McKetta [43], and results are presented next.

Figures 1(a) and (b) show the mole fraction of *n*-hexane in the gas phase, either calculated by the modified Redlich–Kwong equation [41] or the Peng–Robinson equation [23], as a function of pressure at an isotherm of 377.6 K (the critical temperature and pressure of *n*-hexane are 507.4 K and 29.3 atm, respectively). The solid and dashed lines indicate the results by using the comprehensive model (with solubility) and the simplified model (without solubility), respectively. Using the Peng–Robinson equation of state, the experimental data of Poston and McKetta are followed closely. In addition, the two models converge with decreasing ambient pressure as the gas solubility becomes negligible. The Redlich–Kwong equation is

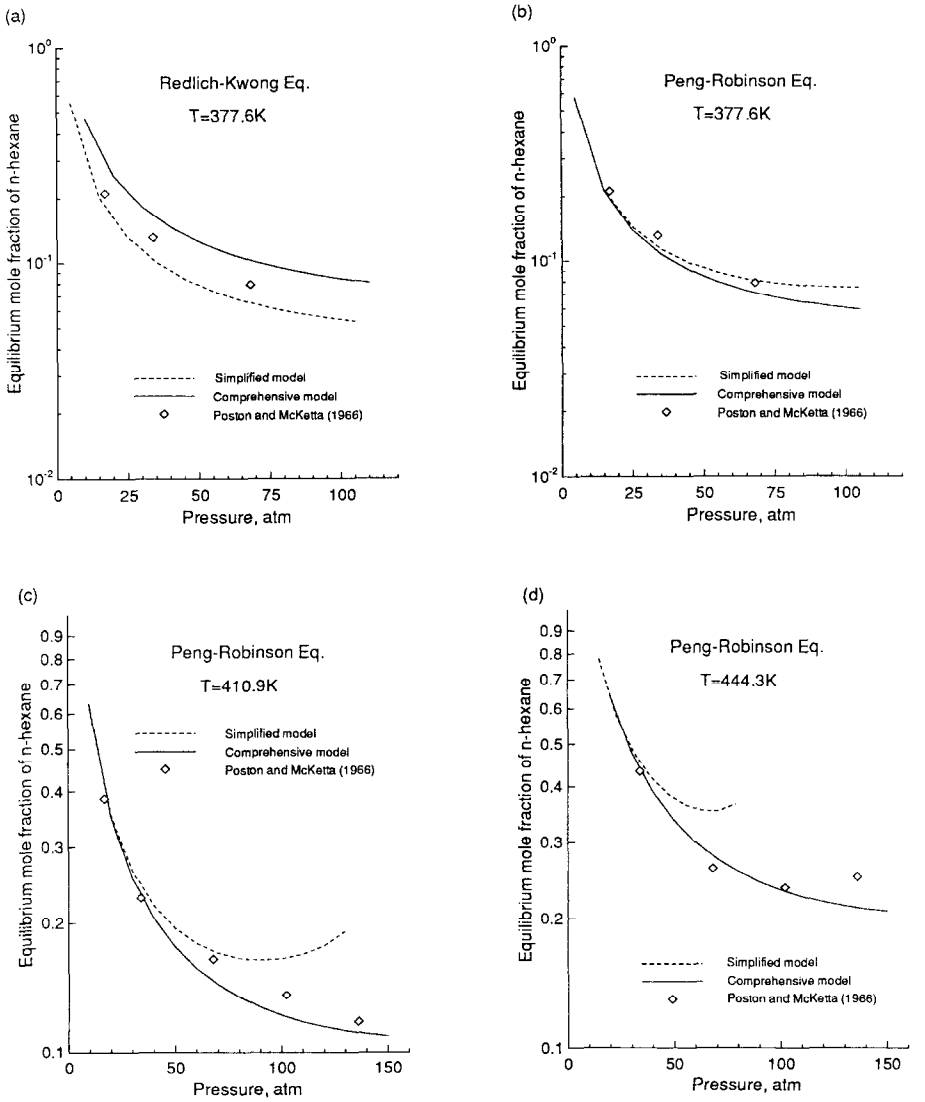

FIG. 1. Mole fraction of *n*-hexane in the gas phase for an *n*-hexane nitrogen system in thermodynamic equilibrium. (a) 377.6 K isotherm with Redlich–Kwong equation, (b) 377.6 K isotherm with Peng–Robinson (PR) equation, (c) 410.9 K isotherm with PR equation, (d) 444.3 K isotherm with PR equation.

shown to be less accurate and the two models differ substantially even at small ambient pressures. Predictions using the Soave–Redlich–Kwong equations are very close to those shown for the Peng–Robinson equation. The Peng–Robinson equation of state has been chosen for all calculations in the present study. In Figs. 1(c) and (d), the mole fraction of *n*-hexane in the gas phase is shown as a function of pressure for higher isotherms (410.9 and 444.3 K). Again, at low pressures, the two models, comprehensive and simplified, are in excellent agreement with the experimental results. However, as the pressure increases, only the comprehensive model remains in agreement with the experimental data. At higher pressures the simplified model starts deviating from the experimental data, and fails to predict the equilibrium composition at high enough pressure. The higher the isotherm, the shorter the range of pressure over which equilibrium composition can be predicted. The simplified model fails at high pressure and temperature because it assumes thermodynamic equilibrium only for the vaporizing species. Consequently, solubility has to be allowed, and the vapor–liquid thermodynamic equilibrium must be considered for both vaporizing and inert species.

Figure 2 shows the energy required for phase change for an *n*-hexane–nitrogen system in equilibrium as a function of temperature for different pressures (30 and 90 atm). Even up to a pressure of 30 atm, the effect of gas solubility on the energy required for phase change is negligible. However, at high pressures, the difference in predicting Δh between the two models increases significantly with temperature.

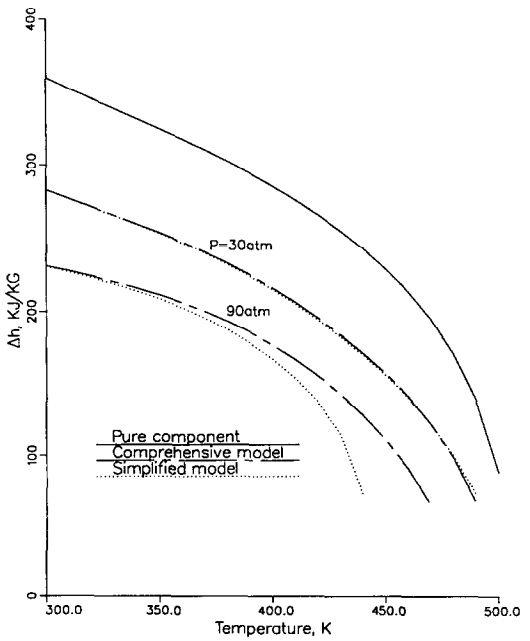

FIG. 2. Gas solubility effect on energy required for phase change for an *n*-hexane–nitrogen system in thermodynamic equilibrium.

When the temperature approaches the critical point of the mixture, an abrupt decrease in Δh occurs. It is also shown that the energy required for phase change for a binary system deviates from the latent heat for pure component substantially with increasing pressure.

Next, results will be presented for an *n*-hexane droplet evaporating into a nitrogen environment ($m_{1,\infty} = 0$) with initial diameter of 100 μm and initial temperature of 300 K.

Figure 3(a) shows the dimensionless droplet lifetime as a function of pressure for three different ambient temperatures (T_∞ = 500, 600 and 750 K). The dimensionless droplet lifetime is given by $\tau\beta/D_0^2$, where τ is the dimensional droplet lifetime, D_0 is the initial droplet diameter and β is the evaporation constant for a droplet evaporating while at its wet-bulb temperature (T_{wb} = 309.5 K), ambient pressure of 1 atm and ambient temperature of 500 K ($\beta = 0.1684$ mm^2 s^{-1}). Results predicted by both models are presented. The comprehensive model is indicated by open circles and the simplified model by diamonds. For T_∞ = 500 K, the two models are in good agreement for ambient pressures up to the critical pressure of pure *n*-hexane. However, at higher ambient pressures, the model that neglects gas solubility deviates significantly from the comprehensive model with increasing pressure. For the highest ambient pressure considered (P_∞ = 100 atm), the model neglecting solubility underpredicts the droplet lifetime by almost 20%. For T_∞ = 600 K, the droplet lifetime predicted by the two models shows similar trends. However, since the model neglecting solubility fails to offer equilibrium composition at high enough pressures and temperatures (see Figs. 1(c) and (d) and the relevant discussion), the droplet lifetime by such a model cannot be obtained for ambient pressures above 70 atm. The higher the ambient temperature, the shorter the ambient pressure range over which the simplified model can be employed. Figure 3(b) presents the droplet lifetime for high ambient temperatures (T_∞ = 1000 and 1500 K). For T_∞ = 1000 and 1500 K, the simplified model can only predict the droplet lifetime up to approximately 40 and 30 atm, respectively. However, it follows the comprehensive model fairly well for the entire range of ambient pressures for which it can provide solutions. Calculations at P_∞ = 100 atm and T_∞ = 1000 K as well as P_∞ = 70 atm and T_∞ = 1500 K were attempted employing the comprehensive model. These calculations were terminated early because the droplet surface reached the critical state. Figure 3(b) also presents results obtained by Hsieh *et al.* [18] for an *n*-pentane droplet evaporating in nitrogen for an ambient temperature of 2000 K. Although direct comparison may be inappropriate because of the different fuel adopted, qualitative agreement between the two studies is definitely suggested in Fig. 3(b).

The droplet lifetime trend with increasing ambient pressure for different ambient temperatures in Fig. 3

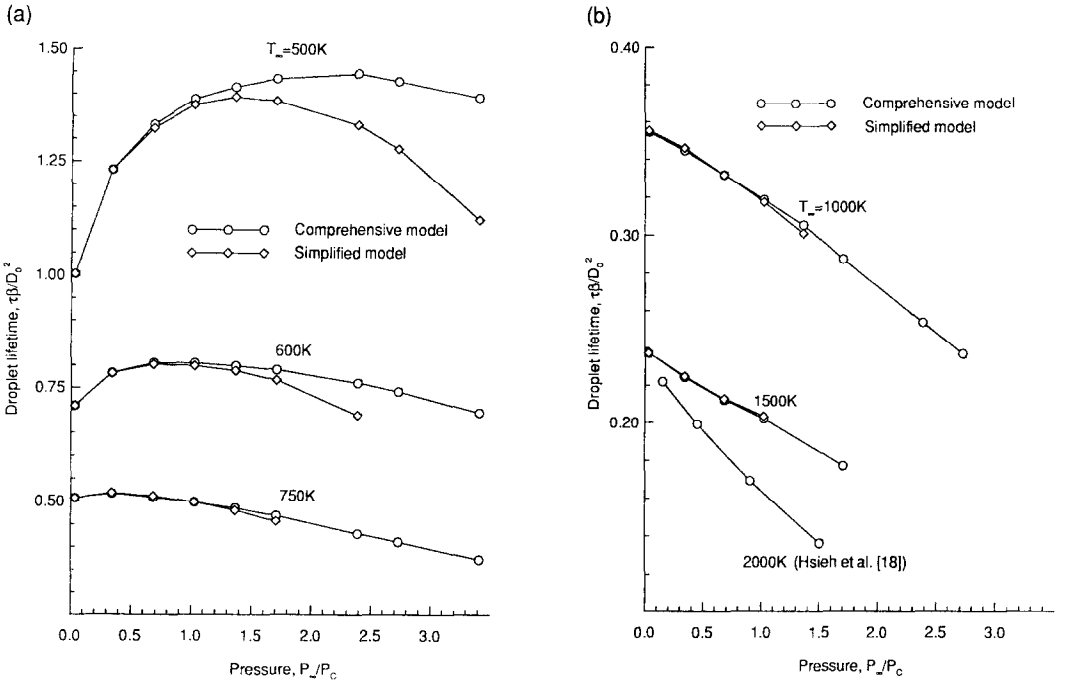

FIG. 3. Dimensionless droplet lifetime with ambient pressure employing both the comprehensive and simplified model. (a) Low and moderate ambient temperatures. (b) High ambient temperatures.

can be explained as follows: with increasing pressure, (i) the droplet heat-up time increases as a proportion of the total vaporization time (see Fig. 5(b) and relevant discussion); (ii) the driving force for heat transferred towards the droplet decreases since the droplet surface temperature increases towards T_∞, and the driving force for mass transfer away from the droplet surface (which, of course, is strongly coupled with the heat transfer problem) decreases since both the binary mass diffusion coefficient and the droplet surface mass fraction of the vaporizing species decrease with increasing pressure (see Fig. 1); and (iii) the energy required for vaporization Δh decreases (see Fig. 2). The latter tends to shorten the droplet lifetime whereas the first two tend to prolong it. It is the competition between these mechanisms that defines the droplet lifetime behavior with increasing pressure for different ambient temperatures [12]. The results in Fig. 3 show that the simplified model can be used for low ambient pressures ($P_\infty < 30$ atm). The accuracy of the calculation is adequate and the complexities and uncertainties a comprehensive model might introduce are avoided. However, for ambient pressures higher than the critical pressure of the pure fuel, only the comprehensive model is applicable and valid.

Figure 4(a) shows the histories of the mass fraction of nitrogen dissolved in the liquid phase at the droplet surface for the ambient temperature of 1000 K at different ambient pressures (10, 40 and 80 atm). For $P_\infty = 10$ atm, the mass fraction of dissolved nitrogen is negligibly small and remains approximately constant over the entire droplet lifetime. Even at an ambient pressure of 40 atm, which is higher than the critical pressure of pure *n*-hexane, the mass fraction of nitrogen is only 2%. However, at 80 atm, the mass fraction of nitrogen at the droplet surface increases progressively with time to a final value of approximately 10%. This corresponds to 25.7% in terms of mole fraction of nitrogen, which is in agreement with values reported by Lazar and Faeth [14] and Hsieh *et al.* [44]. The spatial distribution profiles of nitrogen mass fraction inside the liquid phase as they evolve with time for $P_\infty = 80$ atm and $T_\infty = 1000$ K are shown in Fig. 4(b). It can be seen that mass diffusion inside the liquid phase persists throughout the droplet lifetime ($\tau = 14.08$ ms). Figure 4(c) presents the temperature history at the droplet center and surface for $T_\infty = 1000$ K and $P_\infty = 80$ atm. Under these ambient conditions, no wet-bulb temperature is reached. Both the droplet surface and the center temperature keep increasing until the end of the droplet lifetime. The spatial variation of temperature in the droplet interior for different times is presented in Fig. 4(d). Although the magnitude of the temperature gradient inside the droplet decreases with time, heat-up of the liquid interior persists throughout the entire droplet lifetime.

In Fig. 5(a), the final droplet surface temperature is plotted with ambient pressure. The final temperature is defined as the droplet surface temperature at the end of the transient calculations which are terminated when $(R/R_0)^2 = 0.2$ or the critical mixing point is reached. For the ambient pressures of 100, 120 and 140 atm, the critical mixing temperature was attained. It is shown that it decreases with pressure,

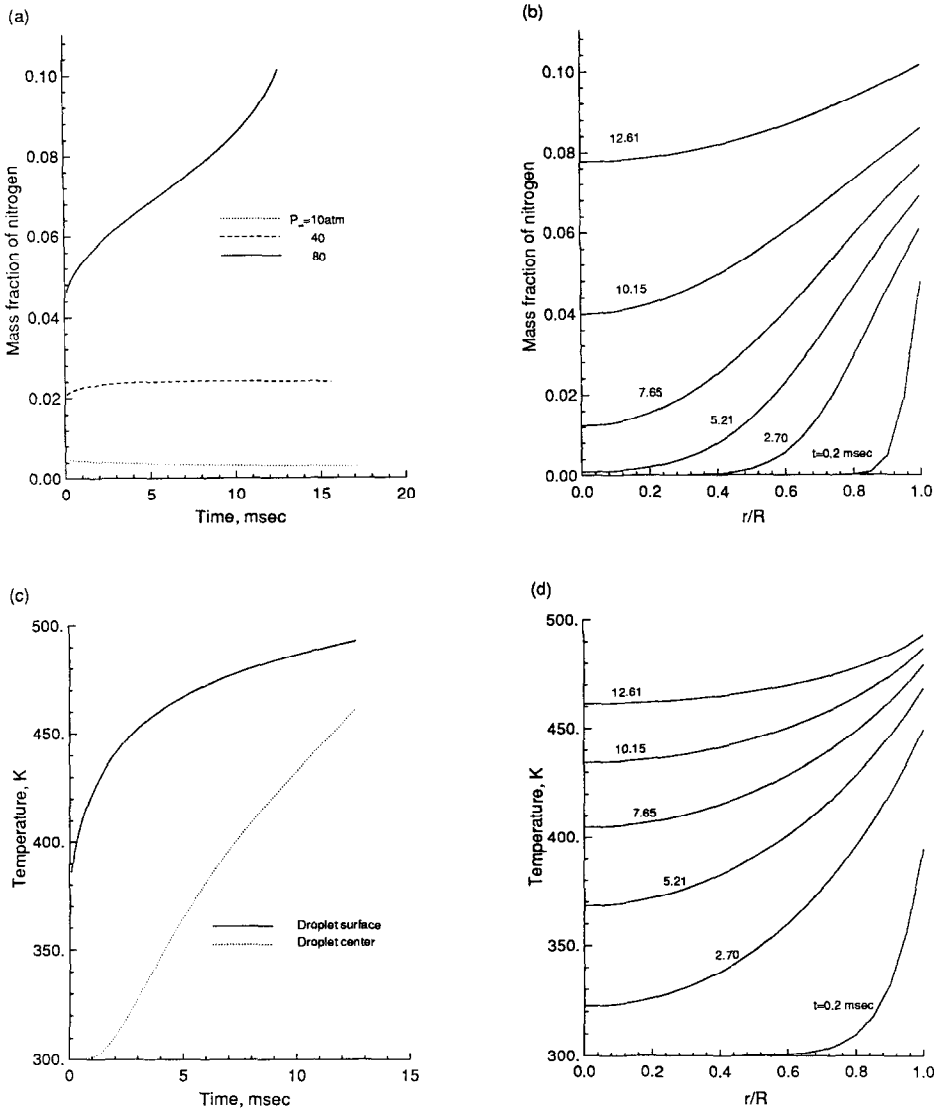

FIG. 4. (a) The histories of the mass fraction of nitrogen dissolved in the liquid phase at the droplet surface for different ambient pressures; $T_\infty = 1000$ K. (b) Spatial and temporal distribution of nitrogen mass fraction in the droplet interior. (c) Temperature history at the droplet center and surface. (d) Spatial and temporal distribution of the temperature in the droplet interior. Ambient conditions for parts (b), (c) and (d): $T_\infty = 1000$ K and $P_\infty = 80$ atm.

which is in agreement with Hsieh *et al.* [18] and Shuen *et al.* [45]. At lower pressures the final droplet surface temperature increases steeply with pressure. Figure 5(b) presents the temporal variation of the ratio of the energy transported into the liquid phase to heat-up the droplet interior, $q_{l,s}$, over that transferred towards the droplet surface from the gaseous phase, $q_{g,s}$ (the difference between the two amounts of energy is utilized for change of phase; see equation (13)). With increasing ambient pressure, the droplet heat-up time increases as a proportion of the total vaporization time. At high enough ambient pressures most of the energy is used to heat-up the droplet interior, since the energy required for phase change decreases with increasing pressure and temperature (see Figs. 2 and 5(a)). Under supercritical conditions the energy required for phase change tends to zero when the critical mixing point is reached. For $P_\infty = 100$ atm the critical mixing temperature is reached when $(R/R_0)^2 = 0.35$. The ratio $q_{l,s}/q_{g,s}$ for this case approaches to unity at that point. It should remain at unity for the remainder of the droplet lifetime, since from that point onwards all energy is used to heat-up the droplet interior. At even higher ambient pressures, the higher the ambient pressure the earlier in the droplet lifetime the critical mixing point is reached. Consequently, heat-up of the droplet interior is expected to be more dominant with further increase in the ambient pressures. In the abscissa in Fig. 5(b) τ is the dimensional droplet lifetime. It is obtained by extrapolating

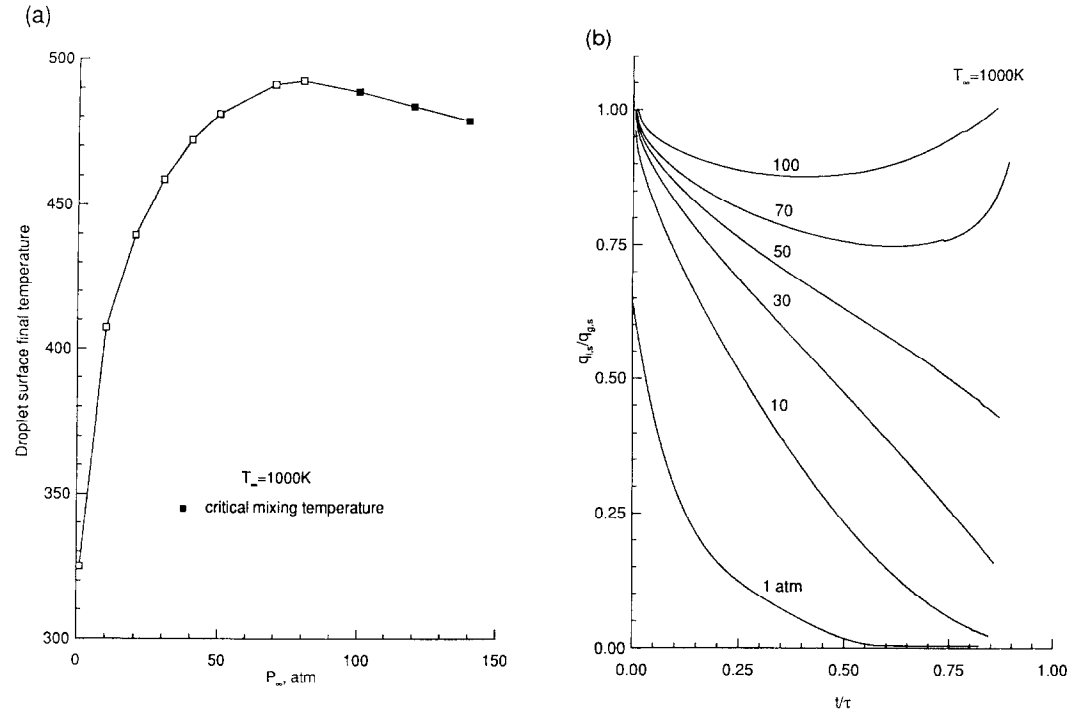

FIG. 5. (a) Droplet surface final temperature with ambient pressure. (b) Interfacial heat transfer variation with time for different ambient pressures.

to zero the temporal variation of $(R/R_0)^2$. In the case of $P_\infty = 100$ atm, τ was obtained similarly, only for plotting convenience. It is realized that beyond the critical mixing point the slope of $(R/R_0)^2$ may change [45].

Figure 6(a) presents the droplet surface temperature as a function of the *n*-hexane mass fraction both in the liquid and gaseous sides of the droplet interface while evolving with time. When the critical point of the binary mixture is reached, there is no distinct transition between the liquid and gas phases. The composition in the liquid phase approaches that

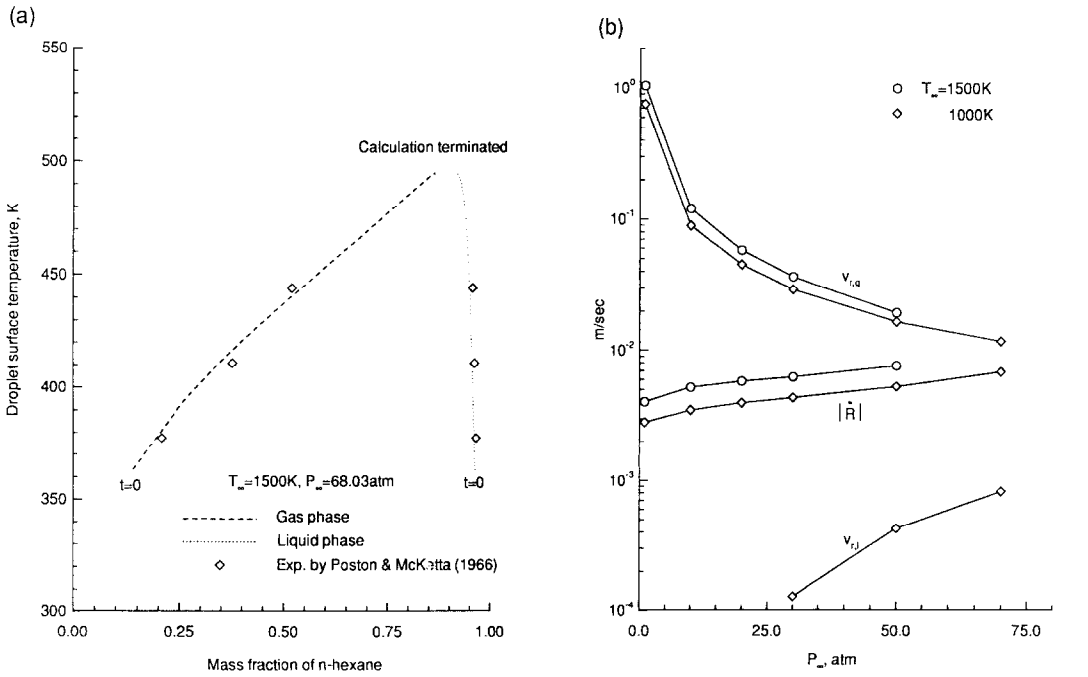

FIG. 6. (a) Droplet surface temperature with *n*-hexane mass fraction both on the liquid and gaseous sides of the droplet interface while evolving with time. (b) Gas- and liquid-phase velocities at the droplet surface and droplet surface regression rate with ambient pressure.

in the gas phase. In this study, we use a rigorous method (see Section 2 for details) to predict the critical point of the binary system. Computations are terminated whenever the droplet surface temperature is a few degrees below the critical temperature. Our predictions in Fig. 6(a) are in excellent agreement with the experimental data of Poston and McKetta [43]. Figure 6(b) presents the droplet surface regression rate, $|\dot{R}|$, and the velocities at the droplet surface $v_{r,g}$ and $v_{r,l}$, on the gas- and liquid-phase sides, respectively, as a function of ambient pressure. These values for $v_{r,g}$, $v_{r,l}$ and $|\dot{R}|$ correspond to the last time-step of the transient calculations which are terminated when $(R/R_0)^2 < 0.2$. At low ambient pressures the ratio $|\dot{R}|/v_{r,g}$ is $O(10^{-2})$, and has been the justification for neglecting the effect of the droplet regression rate in the literature for such pressures. This ratio increases with increasing ambient pressure and becomes $O(1)$ in the proximity of the critical state of the mixture. However, it is mainly the velocity at the droplet surface that decreases dramatically with pressure ($v_{r,g} \propto (1/P_\infty)$) and converges towards $|\dot{R}|$; the droplet regression rate increases merely by a factor of two over this wide range of ambient pressures. The velocity at the droplet surface on the liquid side is negligible at low ambient pressures. As the critical mixing point is reached, the densities in the liquid- and gas-phase sides of the droplet surface approach a single value. Consequently, conservation of mass at the interface (equation (10)), demands that $v_{r,g}$ and $v_{r,l}$ also approach a single value at the critical mixing point. Thus, under supercritical conditions it is expected that the bulk flow in the liquid phase becomes important and the convective terms must be taken into account together with the diffusion processes [45]. However, for conditions even a few degrees below the critical mixing temperature, $v_{r,l}$ remains much smaller than $v_{r,g}$, since densities vary exceedingly fast in the vicinity of the critical mixing point. In the present study, calculations are terminated within a few degrees from the critical mixing point. Furthermore, the liquid phase velocity for spherically symmetric evaporation is maximum at the droplet surface. For these reasons, the convective terms in the liquid phase have been neglected in the present study. However, changes in the liquid phase density both due to thermal expansion and change in species composition have been incorporated in the model and contribute to the rate at which the droplet surface is receding through equation (15). Figure 6(b) shows that for $T_\infty = 1000$ K, even at an ambient pressure of 70 atm, $v_{r,l}$ remains an order of magnitude smaller than $v_{r,g}$.

In Fig. 7, the influence of the ambient mass fraction of the fuel vapor, $m_{l,\infty}$, on droplet evaporation is presented. Calculations were conducted for $m_{l,\infty} = 0.3$ at different ambient temperatures. For high ambient pressures, the initial equilibrium mass fraction of the fuel vapor at the droplet surface is lower than that of the ambient ($m_{l,s} < m_{l,\infty}$). Consequently, the fuel vapor diffuses towards the droplet

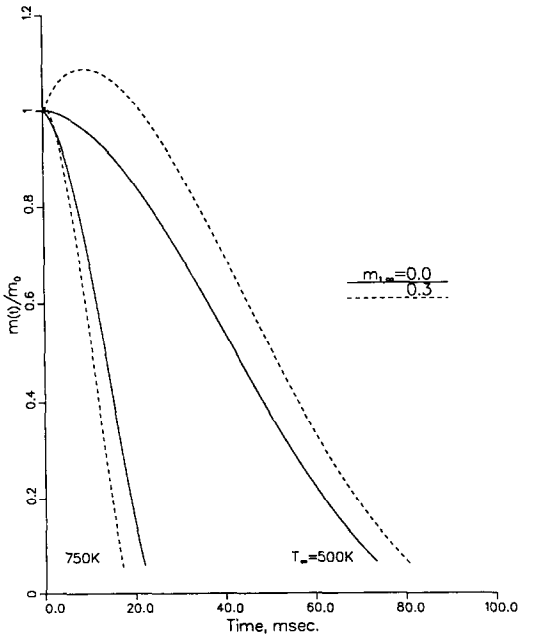

FIG. 7. The history of the dimensionless droplet mass for different ambient temperatures and compositions; $P_\infty = 80$ atm.

surface. Condensation occurs at the droplet surface and the droplet gains mass as a result. Meanwhile, due to the continuous heat flux from the gas phase, the temperature at the droplet surface increases, causing the mass fraction of the fuel vapor at the droplet surface to increase. When $m_{l,s} > m_{l,\infty}$, condensation stops and the droplet starts evaporating. The ratio of the condensation duration to the total droplet lifetime depends on ambient conditions. Figure 7 shows the time history of dimensionless droplet mass for $m_{l,\infty} = 0.0$ and 0.3 at $T_\infty = 500$ K and 750 K with $P_\infty = 80$ atm. For the ambient temperature of 750 K, very little condensation occurs, since large heat flux leads to a rapid increase in surface temperature and the required composition for evaporation is reached within a short time. However, at a lower ambient temperature (500 K), substantial condensation occurs during the early part of the droplet lifetime which increases the droplet mass by almost 10%.

Finally, the necessity to solve the momentum equation simultaneously with the remaining governing equations is examined. Using the ICE technique with pressure gradient scaling, it is predicted that the pressure deviation from the ambient value is negligible; $(P - P_\infty)/P_\infty \leqslant O(10^{-5})$. The maximum $P - P_\infty$ occurs at the droplet surface and decreases with ambient pressures. Calculated values for $P - P_\infty$ are in good agreement with predictions available in ref. [6]. The small pressure deviation suggests that the momentum equation can be decoupled from the remaining set of equations. In this case, under isobaric condition, the radial velocity in the gas phase can be obtained from the continuity equation. The momentum equation can

be used afterwards merely to calculate the pressure field, if so desired. It was found that predictions both for local quantities (flow and temperature fields) and global ones (droplet lifetime) are affected negligibly by including the momentum equation. This is in agreement with Ramshaw *et al.* [22] who concluded that in a low Mach number flow, the pressure gradients are effectively determined by the velocity, and not vice versa.

5. CONCLUSIONS

1. For ambient pressures approximately lower than the critical pressure of the fuel, the droplet lifetimes predicted by either model (simplified and comprehensive) are in agreement.

2. For ambient pressures higher than the critical pressure of the fuel, the simplified model either underestimates the droplet lifetime for low ambient temperatures, or breaks down for high ambient temperatures since it fails to predict equilibrium composition at high enough droplet surface temperatures.

3. The droplet lifetime dependence on ambient pressure and temperature has been predicted. For the range of ambient conditions considered, it presents a maximum at low ambient temperatures and decreases monotonically with pressure at high ambient temperatures.

4. In a fuel rich environment, relatively low ambient temperatures and high ambient pressures condensation occurs at the early part of the droplet lifetime which may increase the droplet mass substantially.

5. The pressure deviation from P_∞ is negligible, making the isobaric assumption valid.

6. At elevated pressures the droplet regression rate $|\dot{R}|$ is of the same magnitude as the gas phase velocity, $v_{r,g}$, at the droplet surface. However, it is mainly $v_{r,g}$ that decreases about two orders of magnitude from its value at 1 atm and converges towards $|\dot{R}|$, which increases merely by a factor of two over this same wide range of ambient pressures. Even at elevated ambient pressures, the bulk flow in the liquid phase may be neglected when the droplet surface temperature is lower than the critical mixing temperature by more than a few degrees. However, under supercritical conditions the liquid phase velocity at the droplet surface, $v_{r,l}$, approaches $v_{r,g}$ and the bulk flow must be taken into account together with the diffusion processes.

7. With increasing ambient pressure, the droplet heat-up time increases as a proportion of the droplet lifetime and becomes extremely important throughout the entire droplet lifetime for high enough ambient pressures.

Acknowledgements—Computational work was performed on the Supercomputer Remote Access and Graphics Center at Rutgers University and the Pittsburgh Supercomputing Center. The support of both computing facilities is greatly appreciated. The authors appreciate the useful suggestions made by the referees.

REFERENCES

1. H. Kawazoe, K. Ohsawa and K. Fujikake, LDA measurement of fuel droplet sizes and velocities in a combustion field, *Combust. Flame* **82,** 151–162 (1990).
2. C. G. McCreath and N. A. Chigier, Liquid-spray burning in the wake of a stabilizer disc, *Fourteenth (International) Symposium on Combustion*, pp. 1355–1363. The Combustion Institute, Pittsburgh (1972).
3. N. A. Chigier and C. G. McCreath, Combustion of droplets in sprays, *Acta Astronautica* **1,** 687–710 (1974).
4. Y. Onuma and M. Ogasawara, Studies on the structure of a spray combustion flame, *Fifteenth (International) Symposium on Combustion*, pp. 453–465. The Combustion Institute, Pittsburgh (1974).
5. E. E. Khalil and J. H. Whitelaw, Aerodynamic and thermodynamic characteristics of kerosene-spray flames *Sixteenth (International) Symposium on Combustion*, pp. 569–576. The Combustion Institute, Pittsburgh (1976).
6. G. M. Faeth, Current status of droplet and liquid combustion, *Prog. Energy Combust. Sci.* **3,** 191–224 (1977).
7. R. L. Matlosz, S. Leipziger and T. P. Torda, Investigation of liquid drop evaporation in a high temperature and high pressure environment, *Int. J. Heat Mass Transfer* **15,** 831–852 (1972).
8. D. E. Rosner, On liquid droplet combustion at high pressures, *AIAA J.* **5,** 163–166 (1967).
9. D. E. Rosner and W. S. Chang, Transient evaporation and combustion of a fuel droplet near its critical temperature, *Combust. Sci. Technol.* **7,** 145–158 (1973).
10. T. Kadota and H. Hiroyasu, Evaporation of a single droplet at elevated pressures and temperatures, *Bull. JSME* **19,** 1515–1521 (1976).
11. J. P. Delplanque and W. A. Sirignano, Transient vaporization and burning for an oxygen droplet at sub- and near-critical conditions, AIAA Paper 91-0075 (1991).
12. H. Jia and G. Gogos, Investigation of liquid droplet evaporation in subcritical and supercritical gaseous environments, *J. Thermophys. Heat Transfer* **6,** 738–745 (1992).
13. J. A. Manrique and G. L. Borman, Calculations of steady state droplet vaporization at high ambient pressures, *Int. J. Heat Mass Transfer* **12,** 1081–1095 (1969).
14. R. S. Lazar and G. M. Faeth, Bipropellant droplet combustion in the vicinity of the critical point, *Thirteenth (International) Symposium on Combustion*, pp. 743–753. The Combustion Institute, Pittsburgh (1971).
15. G. S. Canada and G. M. Faeth, Fuel droplet burning rates at high pressures, *Fourteenth (International) Symposium on Combustion*, pp. 1345–1354. The Combustion Institute, Pittsburgh (1973).
16. E. W. Curtis and P. V. Farrell, Droplet vaporization in a supercritical microgravity environment, *Acta Astronautica* **17,** 1189–1193 (1988).
17. E. W. Curtis and P. V. Farrell, A numerical study of high-pressure droplet vaporization, *Combust. Flame* **90,** 85–102 (1992).
18. K. C. Hsieh, J. S. Shuen and V. Yang, Droplet vaporization in high-pressure environments I: near critical conditions, *Combust. Sci. Technol.* **76,** 111–132 (1991).
19. J. P. Delplanque and W. A. Sirignano, Numerical study of the transient vaporization of an oxygen droplet at sub- and super-critical conditions, *Int. J. Heat Mass Transfer* **36,** 303–314 (1993).
20. F. H. Harlow and A. A. Amsden, A numerical fluid dynamics calculation method for all flow speeds, *J. Comp. Phys.* **8,** 197–213 (1971).
21. C. K. Westbrook, A generalized ICE method for chem-

ically reactive flows in combustion systems, *J. Comp. Phys.* **29,** 67–80 (1978).
22. J. D. Ramshaw, P. J. O'Rourke and L. R. Stein, Pressure gradient scaling method for fluid flow with nearly uniform pressure, *J. Comp. Phys.* **58,** 361–376 (1985).
23. D. Y. Peng and D. B. Robinson, A new two-constant equation of state, *Ind. Engng Chem. Fundam.* **15,** 59–64 (1976).
24. H. Knapp, R. Doring, L. Oellrich, U. Plocker and J. M. Prausnitz, *Vapor–Liquid Equilibria for Mixtures of Low Boiling Substances*, Chemistry Data Series, VI. DECHEMA, Frankfurt a.M. (1982).
25. R. C. Reid, J. M. Prausnitz and B. E. Polling, *The Properties of Gases and Liquids* (4th Edn). McGraw-Hill, New York (1987).
26. R. C. Reid and M. Modell, *Thermodynamics and its Applications* (2nd Edn), p. 227. Prentice-Hall, Englewood Cliffs, NJ (1983).
27. D. Y. Peng and D. B. Robinson, A rigorous method for predicting the critical properties of multicomponent systems from an equation of state, *A.I.Ch.E. Jl* **23,** 137–144 (1977).
28. R. A. Heidemann and A. M. Khalil, The calculation of critical points, *A.I.Ch.E. Jl* **26,** 769–779 (1980).
29. P. D. Neufeld, A. R. Janzen and R. A. Aziz, Empirical equations to calculate 16 of the transport collision integrals $\Omega^{(l,s)}$ for the Lennard–Jones potential, *J. Chem. Phys.* **57,** 1100–1102 (1972).
30. S. Takahashi, Preparation of a generalized chart for the diffusion coefficients of gases at high pressures, *J. Chem. Engng Japan* **6,** 417–420 (1974).
31. T. H. Chung, M. Ajlan, L. L. Lee and K. E. Starling, Generalized multiparameter correlation for nonpolar and polar fluid transport properties, *Ind. Engng Chem. Res.* **27,** 671–679 (1988).
32. T. H. Chung, L. L. Lee and K. E. Starling, Applications of kinetic gas theories and multiparameter correlation for prediction of dilute gas viscosity and thermal conductivity, *Ind. Engng Chem. Fundam.* **23,** 8–13 (1984).
33. L. N. Canjar and F. S. Manning, *Thermodynamic Properties and Reduced Correlation for Gases* (1st Edn), p. 74. Gulf Publishing, Houston, Texas (1967).
34. W. C. Reynolds, *Thermodynamic Properties in SI: Graphs, Tables and Computational Equations for 40 Substances*, p. 54. Stanford University, Stanford (1979).
35. A. Bondi, Estimation of the heat capacity of liquids, *Ind. Engng Chem. Fundam.* **5,** 442–449 (1966).
36. J. S. Rowlingson, *Liquids and Liquid Mixtures* (2nd Edn). Butterworth, London (1967).
37. K. Nakanishi, Prediction of diffusion coefficients of nonelectrolytes in dilute solution based on generalized Hammond–Stokes plot, *Ind. Engng Chem. Fundam.* **17,** 253–256 (1978).
38. L. Riedel, *Chem. Ing. Tech.* **21,** 349 (1949); **23,** 321 & 465 (1951).
39. L. P. Filippov, Thermal conduction of solutions in associated liquids; Thermal conduction of 50 organic liquids, *Chem. Abstr.* **49,** Col. 15430–15431 (1955); **50,** Col. 8276 (1956).
40. S. V. Patankar, *Numerical Heat Transfer and Fluid Flow*, p. 56. Hemisphere, New York (1980).
41. P. L. Chueh and J. M. Prausnitz, Vapor–liquid equilibria at high pressure: vapor-phase fugacity coefficients in nonpolar and quantum-gas mixtures, *I&EC Fundam.* **6,** 492–498 (1967).
42. G. Soave, Equilibrium constants from a modified Redlich–Kwong equation of state, *Chem. Engng Sci.* **27,** 1197–1203 (1972).
43. R. S. Poston and J. J. McKetta, Vapor–liquid equilibrium in the *n*-hexane–nitrogen system, *J. Chem. Engng Data* **11,** 364–365 (1966).
44. K. C. Hsieh, J. S. Shuen and V. Yang, Analysis of multi-component droplet vaporization at near critical conditions, *AIAA* Paper 88-0637 (1988).
45. J. S. Shuen, V. Yang and C. C. Hsiao, Combustion of liquid-fuel droplets in supercritical conditions, *Combust. Flame* **89,** 299–319 (1992).